Acta Cryst E CRYSTALLOGRAPHIC COMMUNICATIONS

ISSN 2056-9890

# 2,2′-(Disulfanediyl)dibenzoic acid *N*,*N*-dimethylformamide monosolvate: crystal structure, Hirshfeld surface analysis and computational study

**Sang Loon Tan‡ and Edward R. T. Tiekink***

Research Centre for Crystalline Materials, School of Science and Technology, Sunway University, 47500 Bandar Sunway, Selangor Darul Ehsan, Malaysia. *Correspondence e-mail: edwardt@sunway.edu.my

Received 18 June 2020
Accepted 22 June 2020

Edited by W. T. A. Harrison, University of Aberdeen, Scotland

‡ Additional correspondence author, e-mail: alant@sunway.edu.my.

**Keywords:** crystal structure; 2,2′-dithiodibenzoic acid; dimethylformamide; hydrogen bonding; Hirshfeld surface analysis; computational chemistry.

**CCDC reference**: 2011285

**Supporting information**: this article has supporting information at journals.iucr.org/e

The title 1:1 solvate, $C_{14}H_{10}O_4S_2{\cdot}C_3H_7NO$, features a twisted molecule of 2,2′-dithiodibenzoic acid (DTBA), with the central C—S—S—C torsion angle being −88.57 (6)°, and a molecule of dimethylformamide (DMF). The carboxylic acid groups are, respectively, close to co-planar and twisted with respect to the benzene rings to which they are connected as seen in the $CO_2/C_6$ torsion angles of 1.03 (19) and 7.4 (2)°. Intramolecular, hypervalent S←O interactions are noted [S···O = 2.6140 (9) and 2.6827 (9) Å]. In the crystal, four-molecule aggregates are formed *via* DTBA-O—H···O(DMF) and DTBA-O—H···O(DTBA) hydrogen bonding, the latter *via* an eight-membered $\{\cdots OHCO\}_2$ homosynthon. These are linked into supramolecular layers parallel to (011) *via* benzene-C—H···O(DTBA) and DTBA-C═O···$\pi$(benzene) interactions, with the connections between these, giving rise to a three-dimensional architecture, being of the type benzene-C—H···$\pi$(benzene). An analysis of the calculated Hirshfeld surfaces indicates, in addition to the aforementioned intermolecular contacts, the presence of stabilizing interactions between a benzene ring and a quasi-$\pi$-system defined by O—H···O hydrogen bonds between a DTBA dimer, *i.e.* the eight-membered $\{\cdots OCOH\}_2$ ring system, and between a benzene ring and a quasi-$\pi$(OCOH···OCH) system arising from the DTBA-O—H···O(DMF) hydrogen bond. The inter-centroid separations are 3.65 and 3.49 Å, respectively.

## 1. Chemical context

Co-crystal formation with 2-mercaptobenzoic acid (2-MBA) is fraught as during crystallization, this is usually oxidized to 2,2′-dithiodibenzoic acid (DTBA) (Broker & Tiekink, 2007; Broker *et al.*, 2008). Indeed, the only co-crystal of 2-MBA is that with DTBA (Rowland *et al.*, 2011). With this chemistry in mind, in recent times it has proved possible to isolate co-crystals of DTBA with other carboxylic acids, such as with a variety of benzoic acid (BA) derivatives, but not always with control over the stoichiometry. Thus, under very much the same conditions, the 1:1 DTBA:BA co-crystal has been characterized (Tan & Tiekink, 2019*a*) along with 2:1 DTBA co-crystals with 3-chlorobenzoic acid (3-ClBA) (Tan & Tiekink, 2019*b*) and the bromo (3-BrBA) analogue (Tan & Tiekink, 2019*c*). The common supramolecular feature of these crystals is the formation of eight-membered $\{\cdots HOCO\}_2$ synthons, occurring between like and/or unlike carboxylic acids. In a recent study, it was found the anticipated $\{\cdots HOCO\}_2$ synthon was not always formed but was usurped by a DTBA-O—H···O(DMF) hydrogen bond for one of the carboxylic acids, *i.e.* in the 1:1:1 co-crystal solvate DTBA:2-ClBA:DMF (Tan & Tiekink, 2019*d*); DMF is dimethylformamide. It turns out the

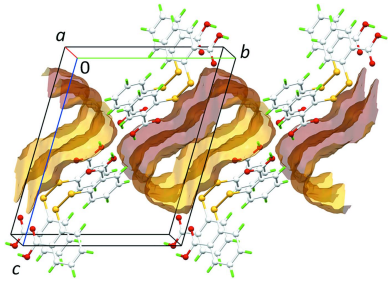

same situation is noted in the structure of the DTBA:2DMF solvate (Cai *et al.*, 2006; Ma *et al.*, 2013; Baruah, 2016) where the DMF molecule effectively blocks off the capacity for $\{\cdots HOCO\}_2$ synthon formation by DTBA. In our hands, recrystallization of 2-MBA from a benzene/DMF (1 ml/7 ml *v*/*v*) solution also gave the DTBA:2DMF solvate (Tan & Tiekink, 2020). However, an analogous experiment from a benzene/DMF (5 ml/1 ml *v*/*v*) solution yielded the mono-solvate, *i.e.* the title compound DTBA:DMF, (I). The crystal and molecular structures of (I) are described herein along with an analysis of the calculated Hirshfeld surfaces and a computational chemistry study.

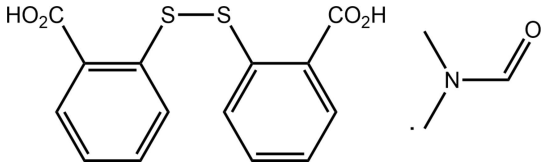


## 2. Structural commentary

The asymmetric unit of (I) comprises a molecule of dithiodibenzoic acid (DTBA) and dimethylformaide (DMF), each in a general position, Fig. 1. The crystals were obtained from the recrystallization of 2-mercaptobenzoic acid from a benzene/DMF (5 ml/1 ml *v*/*v*) solution indicating the acid oxidized to DTBA during crystallization. The observed disparity in the C—O bond lengths in the carboxylic acid residues [C1—O1,O2 = 1.3177 (15) & 1.2216 (15) Å and C14—O3,O4 = 1.3184 (14) & 1.2295 (14) Å] confirms the location of the acidic H atoms on the O1 and O3 atoms, respectively. A characteristic twisted conformation is evidenced in the C3—S1—S2—C8 torsion angle of −88.57 (6)°. The dihedral angle between the benzene rings is 87.71 (3)°, consistent with an orthogonal disposition. The C1-carboxylic acid group is almost co-planar with the (C2–C7) benzene ring to which it is connected with the dihedral angle between the least-squares planes being 1.03 (19)°. By contrast, a small twist is noted for the C14-carboxylic acid residue where the comparable dihedral angle is 7.4 (2)°. Intramolecular hypervalent S←O interactions (Nakanishi *et al.*, 2007) are indicated as the carbonyl-O2 and O4 atoms are orientated towards the disulfide-S1 and S2 atoms, respectively, with the S1···O2 and S2···O4 separations being 2.6140 (9) and 2.6827 (9) Å, respectively.

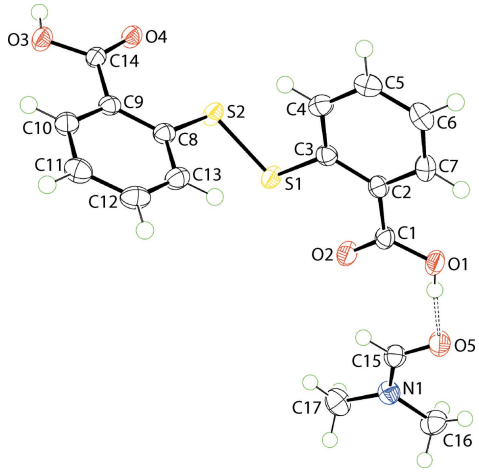


**Figure 1**
The molecular structures of the constituents of (I) showing the atom-labelling scheme and displacement ellipsoids at the 70% probability level. The dashed line indicates a hydrogen bond.

**Table 1**
Hydrogen-bond geometry (Å, °).

*Cg*1 and *Cg*2 are the centroids of the (C2–C7) and (C8–C13) rings, respectively.

| *D*—H···*A* | *D*—H | H···*A* | *D*···*A* | *D*—H···*A* |
|---|---|---|---|---|
| O1—H1*O*···O5 | 0.85 (1) | 1.75 (1) | 2.5981 (13) | 176 (2) |
| O3—H3*O*···O4$^{i}$ | 0.84 (2) | 1.78 (2) | 2.6215 (13) | 175 (2) |
| C15—H15···O2 | 0.95 | 2.38 | 3.1162 (15) | 134 |
| C7—H7···O1$^{ii}$ | 0.95 | 2.53 | 3.2850 (16) | 136 |
| C1—O2···*Cg*1$^{iii}$ | 1.22 (1) | 3.42 (1) | 3.4843 (12) | 83 (1) |
| C14—O4···*Cg*2$^{iv}$ | 1.23 (1) | 3.33 (1) | 3.6227 (12) | 94 (1) |
| C11—H11···*Cg*1$^{v}$ | 0.95 | 2.94 | 3.7962 (14) | 150 |

Symmetry codes: (i) $-x-1, -y+2, -z$; (ii) $-x, -y+1, -z+1$; (iii) $x+1, y, z$; (iv) $x-1, y, z$; (v) $-x, -y+1, -z$.

## 3. Supramolecular features

The key feature of the supramolecular aggregation in the crystal of (I) is the formation of hydrogen bonds between the DTBA-hydroxyl-O1 and the DMF-O5 atoms, as indicated in Fig. 1 and detailed in Table 1, along with hydrogen bonds between centrosymmetrically related C14-carboxylic acid groups associating *via* an eight-membered $\{\cdots OHCO\}_2$ homosynthon. The result is the four-molecule aggregate shown in Fig. 2(*a*). For the DTBA···DMF interaction, further stabilization is realized through a DMF-C15—H···O2(carbonyl) contact, Table 1, to close a seven-membered $\{\cdots HOCO\cdots HCO\}$ heterosynthon. This cooperativity accounts for the near co-planar relationship between the C1-carboxylic acid group and the non-H atoms of the DMF molecule (r.m.s. deviation = 0.0125 Å) as seen in the dihedral angle of 10.21 (19)° between the two residues. The four-molecule aggregates are linked into supramolecular chains *via* benzene-C7—H···O(hydroxyl) interactions occurring between centrosymmetrically related molecules. The chains are connected by parallel C═O···$\pi$(benzene) interactions as detailed in Fig. 2(*b*) and Table 1. The resulting supramolecular layer is parallel to (011), Fig. 2(*c*), with connections between them leading to a three-dimensional architecture being benzene-C11—H···$\pi$(benzene), Fig. 2(*d*).

Crystal (I) was also subjected to the calculation of solvent-accessible void space through *Mercury* (Macrae *et al.*, 2020) with a probing radius of 1.2 Å within an approximate grid spacing of 0.3 Å. It was found that the DMF solvent molecules occupy about 25.4% or equivalent to 220.8 Å$^3$ of the unit-cell volume, whereas the remaining 74.6% or equivalent to

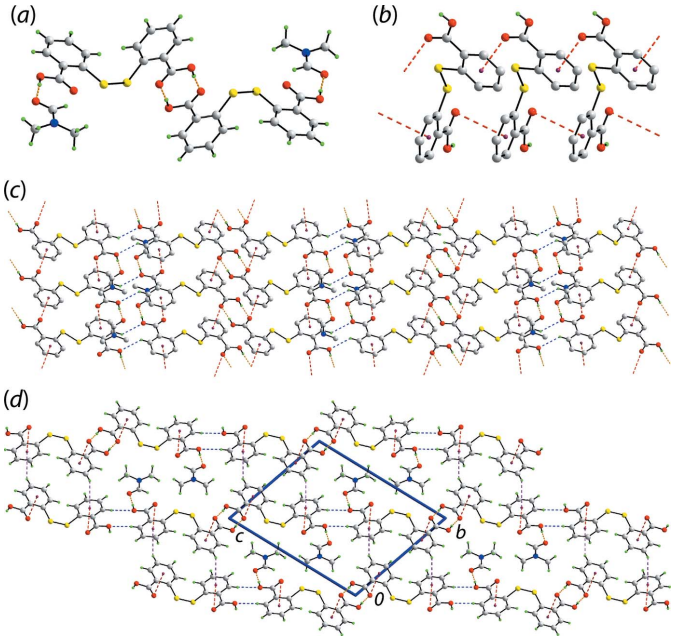


**Figure 2**
Molecular packing in the crystal of (I): (*a*) the four-molecule aggregate sustained by DTBA-O—H···O(DMF) and DTBA-O—H···O(DTBA) hydrogen bonding shown as orange dashed lines, (*b*) the supramolecular chain sustained by carbonyl-O···$\pi$(benzene) interactions shown as red dashed lines, (*c*) the supramolecular layer with benzene-C—H···O(DTBA) interactions shown as blue dashed lines and (*d*) a view of the unit-cell contents down the *a* axis with benzene-C—H···$\pi$(benzene) interactions shown as purple dashed lines. In (*b*) and (*c*) the non-participating H atoms have been omitted to aid clarity.

649.2 Å$^3$ is occupied by DTBA molecules, as highlighted in Fig. 3.

## 4. Hirshfeld surface analysis

To better comprehend the supramolecular features of (I), it was subjected to Hirshfeld surface analysis through *Crystal Explorer 17* (Turner *et al.*, 2017) using the established methods (Tan *et al.*, 2019). Several close contacts with distances shorter than the sum of van der Waals radii (Spackman & Jayatilaka, 2009) are manifested by red spots of varying intensities on the Hirshfeld surface calculated over $d_{norm}$ in Fig. 4. Specifically, the most intense red spots are noted for hydroxy-O1—

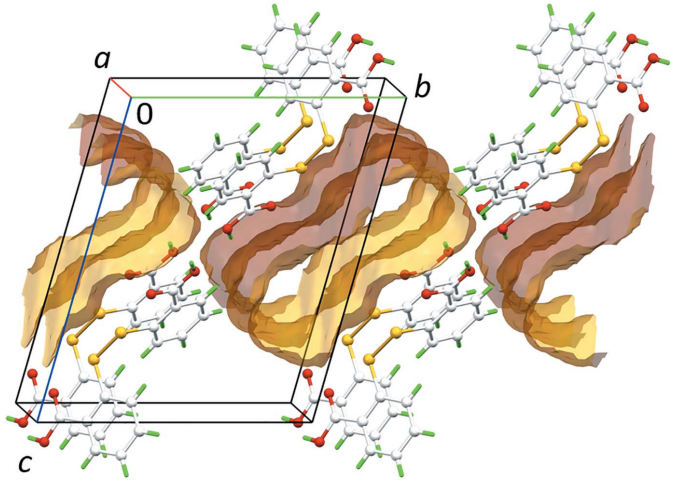


**Figure 3**
A perspective view of the solvent-accessible voids in the crystal of (I), calculated after removal of the DMF solvent molecules within 2 × 2 × 1 unit-cells.

**Table 2**
A summary $d_{norm}$ contact distances (adjusted to neutron values) for interactions present in the crystal of (I) as computed through a Hirshfeld surface analysis.

| Contact | Distance | ΣvdW[a] | Δ\|($d_{norm}$ − ΣvdW)\| | Symmetry operation |
|---|---|---|---|---|
| H1*O*···O5[b] | 1.62 | 2.61 | 0.99 | *x*, *y*, *z* |
| H3*O*···O4[b] | 1.64 | 2.61 | 0.97 | −1 − *x*, 2 − *y*, −*z* |
| O2···H15 | 2.29 | 2.61 | 0.32 | *x*, *y*, *z* |
| H7···O1 | 2.44 | 2.61 | 0.17 | −*x*, 1 − *y*, 1 − *z* |
| H5···C11 | 2.64 | 2.79 | 0.15 | −1 − *x*, 1 − *y*, − *z* |
| H11···C6 | 2.66 | 2.79 | 0.13 | −*x*, 1 − *y*, −*z* |
| C1···C15 | 3.28 | 3.40 | 0.12 | −1 + *x*, *y*, *z* |
| H6···O5 | 2.49 | 2.61 | 0.12 | −*x*, 1 − *y*, 1 − *z* |
| H11···C5 | 2.68 | 2.79 | 0.11 | −*x*, 1 − *y*, −*z* |
| O4···H16*A* | 2.53 | 2.61 | 0.08 | 1 − *x*, 2 − *y*, 1 − *z* |
| O3···C14 | 3.17 | 3.22 | 0.05 | −*x*, 2 − *y*, −*z* |
| C14···C14 | 3.37 | 3.40 | 0.03 | −*x*, 2 − *y*, −*z* |

Notes: (*a*) ΣvdW is the sum of the respective van der Waals radii; (*b*) these interactions correspond to conventional hydrogen bonds.

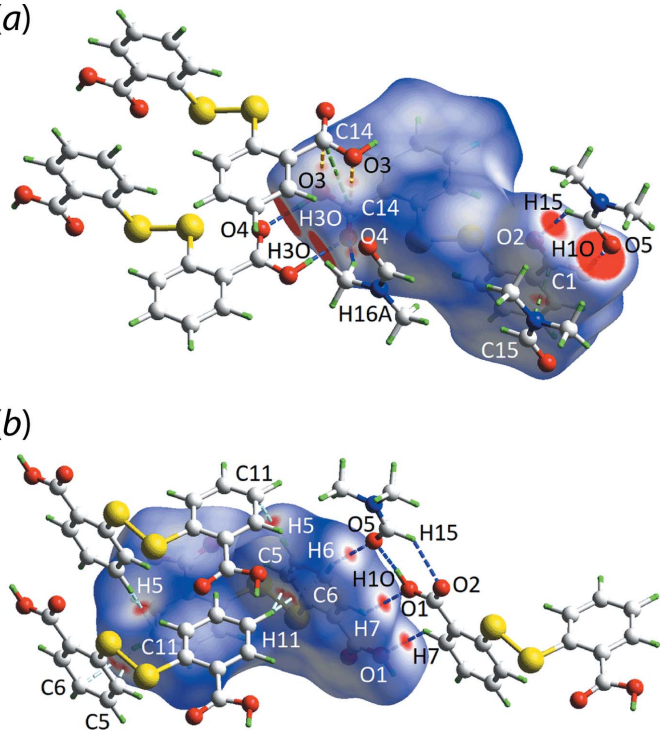


**Figure 4**
Two views of the $d_{norm}$ map for the DTBA molecule, showing the relevant short contacts indicated by the red spots on the Hirshfeld surface with varying intensities within the range of −0.0140 to 1.0154 arbitrary units for (*a*) H3*O*···O4, H1*O*···O5, H15···O2, C15···C1, C14···O3, C14···C14 and H16*A*···O4 and (*b*) H6···O5, H7···O1, H5···C11, H11···C5 and H11···C6. All H···O/O···H interactions are indicated in blue, H···C/C···H in light-blue, C···O/O···C in yellow and C···C in green. The close contacts present in the DMF molecule mirror that of the DTBA and hence the relevant $d_{norm}$ maps are not shown.

H1*O*···O5(carbonyl) and hydroxy-O3—H3*O*···O4(carbonyl) hydrogen bonds with the corresponding $d_{norm}$ contact distances being 1.62 and 1.64 Å, respectively, *i.e.* significantly shorter by almost 1 Å compared to the sum of the van der Waals radii of 2.61 Å (adjusted to neutron values), Table 2. Red spots of moderate intensity are observed for DMF-C15—H15···O2(carbonyl) contact with a distance of 2.29 Å, while spots with weak to diminutive intensities are observed for other close contacts which mainly involve the aromatic rings and carboxylic groups of DTBA as well as the carbonyl group of DMF.

Of particular interest among all close contacts present in (I) is a O3···C14 interaction, which is included within an apparent $\pi$–$\pi$ interaction formed between the C8–C13 benzene ring and a quasi-$\pi$-system defined by O3—H3*O*···O4 hydrogen bonds between a DTBA dimer, *i.e.* the eight-membered $\{\cdots$O4–C14–O3–H3*O*$\}_2$ ring system. A similar observation is also noted for the C1···C15 contact which is encapsulated within an apparent $\pi$(C2–C7)···quasi-$\pi$(O2–C1–O1–H1*O*···O5–C15–H15) interaction. The separation between the ring centroids of the aforementioned $\pi$–$\pi$ contacts are 3.65 and 3.49 Å, respectively. The stacking arrangement between the relevant aromatic and quasi-aromatic rings is supported by shape complementarity as revealed by the concave (red) and convex (blue) regions in the shape index, Fig. 5(*a*)–(*d*), as well as curvedness mappings, Fig. 5(*e*) and (*f*), obtained through the Hirshfeld surface analysis.

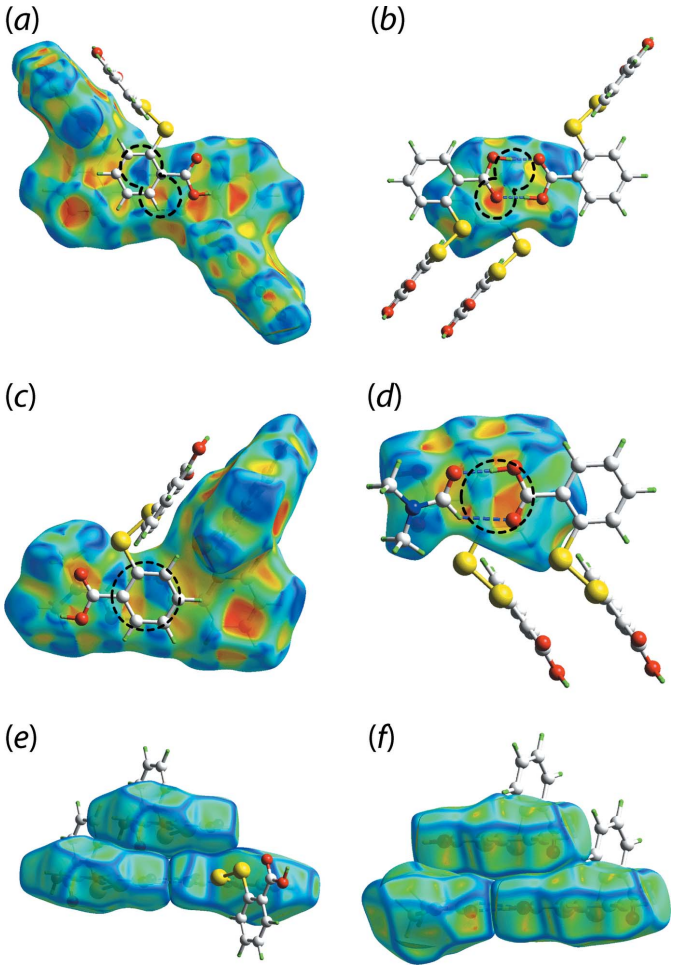


**Figure 5**
The Hirshfeld surface mapped with shape index (property range: −1.0 to +1.0 arbitrary units) for (*a*) a DTBA dimer, (*b*) a benzoic acid fragment in the opposite view of the DTBA dimer shown in (*a*), (*c*) a DTBA···DMF dimer and (*d*) a benzoic acid fragment in the opposite view of the DTBA···DMF dimer shown in (*c*). The Hirshfeld surface mapped with curvedness (property range: −4.0 to +0.4 arbitrary units) for the (*e*) $\pi$(C8–C13)···quasi-(···O4–C14–O3–H3*O*)$_2$ interaction and (*f*) $\pi$(C2–C7)···quasi-(O2–C1–O1–H1*O*···O5–C15–H15) interaction. Both shape index and curvedness studies reveal the shape complementarity (as circled for the concave and convex represented by the red and blue regions in shape index) for the stacking arrangements between the corresponding ring systems.

**Table 3**
Electrostatic potential charge ($V_{ESP}$) for each hydrogen-atom donor and acceptor in (I) participating in a close contact identified through the Hirshfeld surface analysis.

| Contact | Electrostatic potential, $V_{ESP}$ (a.u.) | | $\Delta\lvert V_{ESP}\rvert$ |
|---|---|---|---|
| | H-donor | H-acceptor | |
| H1*O*···O5 | 0.2757 | −0.0854 | 0.3611 |
| H3*O*···O4 | 0.2622 | −0.0476 | 0.3098 |
| H6···O5 | 0.0394 | −0.0875 | 0.1269 |
| H16*A*···O4 | 0.0366 | −0.0669 | 0.1035 |
| H15···O2 | 0.0362 | −0.0605 | 0.0967 |
| H7···O1 | 0.0373 | −0.0249 | 0.0622 |
| H11···C6 | 0.0465 | −0.0080 | 0.0545 |
| H11···C5 | 0.0431 | −0.0068 | 0.0499 |
| H5···C11 | 0.0446 | −0.0016 | 0.0462 |
| C14···O3 | 0.0192 | −0.0080 | 0.0272 |
| C1···C15 | 0.0238 | 0.0161 | 0.0077 |
| C14···C14 | 0.0196 | 0.0191 | 0.0005 |

The electrostatic potential property was mapped onto the Hirshfeld surface using the DFT-B3LYP/6-31G(*d*,*p*) approach to verify the nature of the contacts present in (I). The electrostatic charges for the points of contacts between each H-atom donor and acceptor are collated in Table 3. The results show that those interactions involving H-donors and O-acceptors are electrostatic in nature owing to the relatively great charge disparity between interacting atoms, with the greatest disparity being observed for the H1*O*···O5 followed by H3*O*···O4 interactions which is consistent with their corresponding short contact distances. By contrast, for the H···C and C···O interactions relatively smaller charge disparity is noted indicating weaker attractions between the participating atoms,. The exception is found for the C···C contacts which exhibit positive electrostatic charge for both donor and acceptor atoms signifying the dispersive nature of the contacts.

The quantification of the corresponding close contacts on the Hirshfeld surface through fingerprint plot analysis for overall (I) and its individual components, Fig. 6, show that the distributions mainly comprise H···H [(I): 38.8%; DTBA: 34.8%; DMF: 42.7%], H···O/O···H [(I): 20.9%; DTBA: 21.5%; DMF: 33.7%], H···C/C···H [(I): 16.3%; DTBA: 18.8%; DMF: 6.1%] and H···S/S···H [(I): 11.3%; DTBA: 9.7%; DMF: 13.7%]. The distinctive peaks of the minimum $d_i + d_e$ values for H···O/O···H contacts correspond to O1—

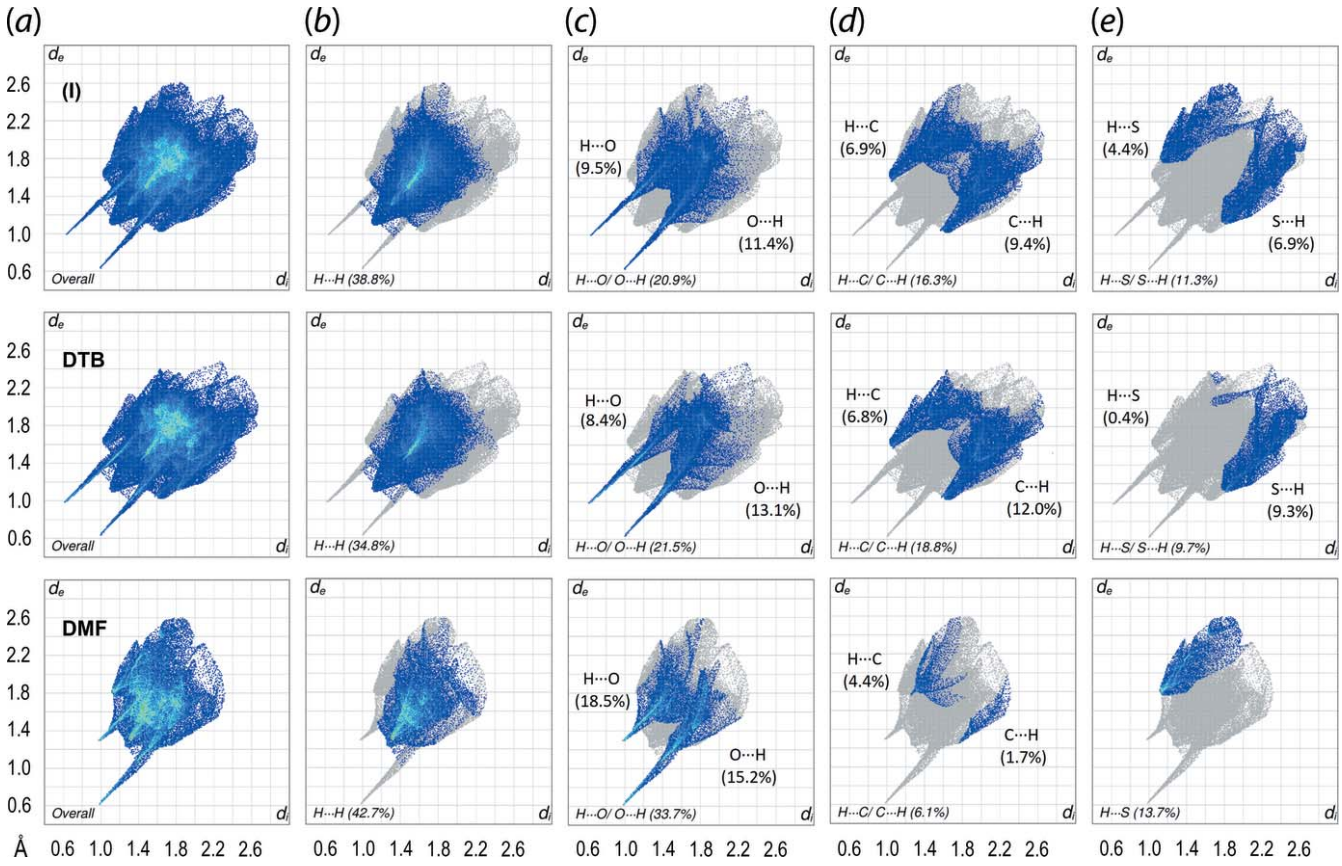


**Figure 6**
(*a*) The overall two-dimensional fingerprint plots for (I) (upper view), DTBA (middle) and DMF (lower) showing the corresponding overall fingerprint profiles as well as those delineated into (*b*) H···H, (*c*) H···O/ O···H, (*d*) H···C/ C···H and (*e*) H···S/ S···H contacts, with the percentage contributions being specified for each contact indicated therein.

H1*O*···O5, O3—H3*O*···O4 and C15—H15···O2, and for the H···C/C···H contacts, to C5—H5···C11 and C11—H11···C6, while the peaks for H···S/ S···H exhibit a $d_i + d_e$ contact distance of ∼2.92 Å, which is slightly shorter than the sum of the van der Waals radii (∑vdW radii) of 2.89 Å, Fig. 6(*e*). Further delineation of H···O/O···H, H···C/C···H and H···S/S···H shows that those heterogeneous contacts are more inclined towards (internal)-*X*···H-(external) in DTBA, while the opposite is true for DMF indicating the complementary H-bond accepting and donating nature of DTBA and DMF, respectively. The inclination is more towards (internal)-*X*···H-(external) for (I) which reflects the relatively small exposed surface for the DMF molecule and limited hydrogen-bond donating role in the overall molecular packing.

## 5. Computational chemistry

The program *NCIPLOT* (Johnson *et al.*, 2010) was employed to verify the non-covalent contacts for the π(C8–C13)–quasi-π(···O4–C14–O3–H3*O*)$_2$ and π(C2–C7)–quasi-π(O2–C1–O1–H1*O*···O5–C15–H15) interactions as detected in the Hirshfeld surface analysis by calculating the electron density derivatives through wavefunction approach. The visualization of the resulting gradient isosurface supported the existence of the π–quasi-π contacts based on the corresponding large green domain sandwiched between the aromatic and quasi-aromatic rings. The overall density is in the range of $-0.05 < \mathrm{sign}(\lambda^2)\rho < 0.03$ a.u. indicating a weak but attractive interaction (Contreras-García *et al.*, 2011), Fig. 7.

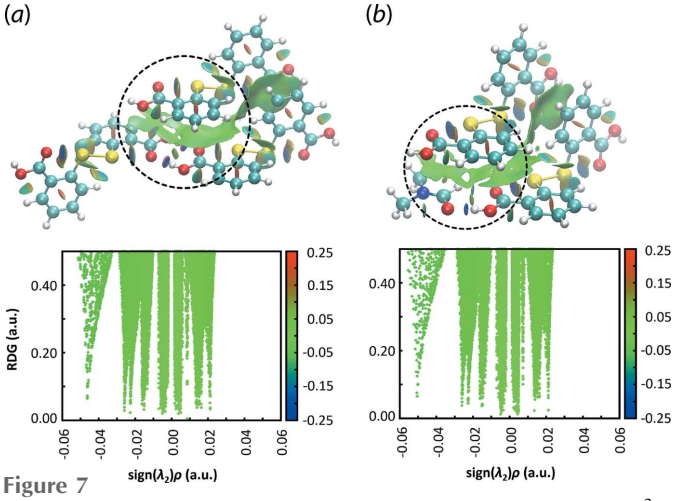


**Figure 7**
The non-covalent interaction and corresponding RDG versus $\mathrm{sign}(\lambda^2)\rho$ plots for the (*a*) π(C8–C13)···quasi-(···O4–C14–O3–H3*O*)$_2$ interaction and (*b*) π(C2–C7)···quasi-(O2–C1–O1–H1*O*···O5–C15–H15) interaction. Both interactions are circled in black.

**Table 4**
A summary of interaction energies (kJ mol$^{-1}$) calculated for (I).

| Contact | $E_{ele}$ | $E_{pol}$ | $E_{dis}$ | $E_{rep}$ | $E_{tot}$ | symmetry operation |
|---|---|---|---|---|---|---|
| {O3—H3*O*···O4}$_2$ | −135.2 | −21.5 | −12.1 | 99.1 | −69.8 | $-1-x, 2-y, -z$ |
| O1—H1*O*···O5 + | | | | | | |
| C15—H15···O2 | −94.8 | −15.8 | −9.5 | 61.3 | −58.9 | $x, y, z$ |
| {C11—H11···$\pi$(C2–C7)}$_2$ | −10.6 | −0.8 | −30.5 | 17.7 | −24.2 | $-x, 1-y, -z$ |
| {C14···O3}$_2$ + | | | | | | |
| C14···C14 | −7.0 | −1.2 | −20.3 | 7.1 | −21.5 | $-x, 2-y, -z$ |
| C1···C15 | −6.4 | −2.1 | −18.5 | 7.0 | −19.9 | $-1+x, y, z$ |
| C16—H16*A*···O4 | −9.9 | −1.6 | −12.5 | 9.5 | −14.6 | $1-x, 2-y, 1-z$ |
| {C5—H5···$\pi$(C8–C13)}$_2$ | −6.0 | −0.6 | −22.6 | 12.1 | −14.2 | $-1-x, 1-y, -z$ |
| C6—H6···O5 | −7.0 | −2.0 | −19.7 | 3.0 | −9.5 | $-x, 1-y, 1-z$ |
| C7—H7···O1 | −3.8 | −0.8 | −12.6 | 10.1 | −7.2 | $-x, 1-y, 1-z$ |

The strength of each close contact between all pairwise molecules in (I) was quantified through the calculation of the interaction energies using *Crystal Explorer 17* (Turner *et al.*, 2017). As expected, the conventional hydroxy-O3—H3*O*···O4(carbonyl) hydrogen bond, leading to the eight-membered homosynthon as well as the seven-membered heterosynthon formed between hydroxy-O1—H1*O*···O5(carbonyl) and DMF-C15—H15···O2(carbonyl) exhibit the greatest interaction energies ($E_{int}$) of −69.8 and −58.9 kJ mol$^{-1}$, respectively. These are relatively stronger than the other supplementary contacts in (I), in which the corresponding energy terms, *viz*. electrostatic ($E_{ele}$), polarization ($E_{pol}$), dispersion ($E_{dis}$), exchange-repulsion ($E_{rep}$) together with the total energy are collated in Table 4.

Complementing the calculations with *Crystal Explorer* 17, the $E_{int}$ for the pairs of $\pi$···quasi-$\pi$ interactions were modelled in *Gaussian16* (Frisch *et al.*, 2016) by subjecting the respective three-molecule aggregates as well as the hydrogen-bonded dimers, as shown in Fig. 7, for gas-phase energy calculation through a long-range corrected $\omega$B97XD functional combining the D2 version of Grimme's dispersion model (Chai & Head-Gordon, 2008) and coupled with Ahlrichs's valence triple-zeta polarization basis sets ($\omega$B97XD/def2-TZVP) (Weigend & Ahlrichs, 2005). Counterpoise methods (Boys & Bernardi, 1970; Simon *et al.*, 1996) were applied to correct for basis set superposition error (BSSE) in the obtained energies. The corresponding three-molecule aggregates exhibit the greatest stabilization energy with the $E$ being −132.5 and −119.7 kJ mol$^{-1}$, respectively, which is consistent with the large localized green domains as detected through *NCIPLOT*. Upon the subtraction of the $E$ contributed by the hydrogen bonded dimers, *i.e.* −73.2 kJ mol$^{-1}$ for {···OCOH}$_2$ and −60.5 kJ mol$^{-1}$ for {···OCOH···OCH}, the remaining energies are ascribed to the $\pi$(C8–C13)···quasi-$\pi$(···O4–C14–O3–H3*O*)$_2$ or $\pi$(C2–C7)···quasi-$\pi$(O2–C1–O1–H1*O*···O5–C15–H15) interactions, *i.e.* −59.3 and −59.2 kJ mol$^{-1}$, respectively.

The crystal of (I) is predominantly governed by electrostatic force attributed to the strong O—H···O hydrogen-bonding contacts that lead to a maze-like $E_{ele}$ topological framework as shown in Fig. 8(*a*). On the other hand, the dispersion force sustained by the specified $\pi$–$\pi$ interactions results in a boat-shape topology, Fig. 8(*b*). The combination of the electrostatic and dispersion forces supersedes the strong interaction energy from O—H···O contacts and lead to a refined overall energy framework with razor-blade-like topology, Fig. 8(*c*).

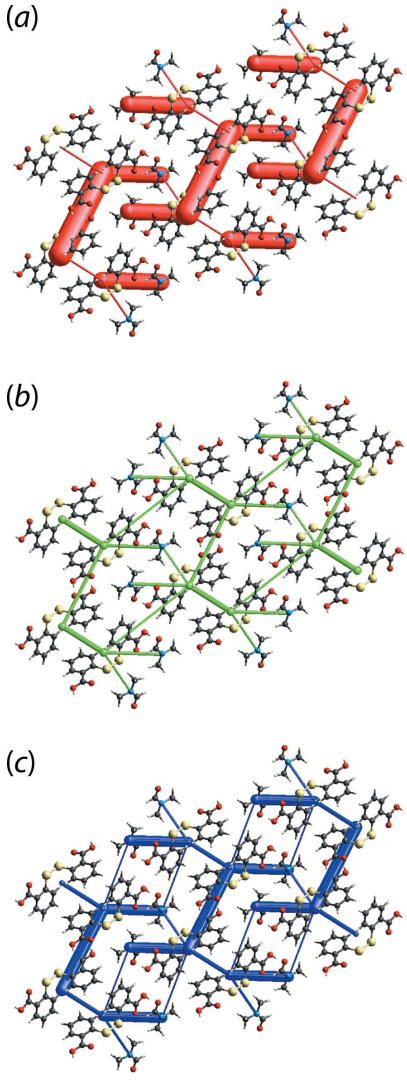


**Figure 8**
The energy frameworks for (I) viewed along the *a* axis, showing the (*a*) electrostatic force, (*b*) dispersion force and (*c*) total energy diagram. The cylindrical radius is proportional to the relative strength of the corresponding energies and they were adjusted to the same scale factor of 100 with a cut-off value of 8 kJ mol$^{-1}$ within a 2 × 2 × 2 unit cells.

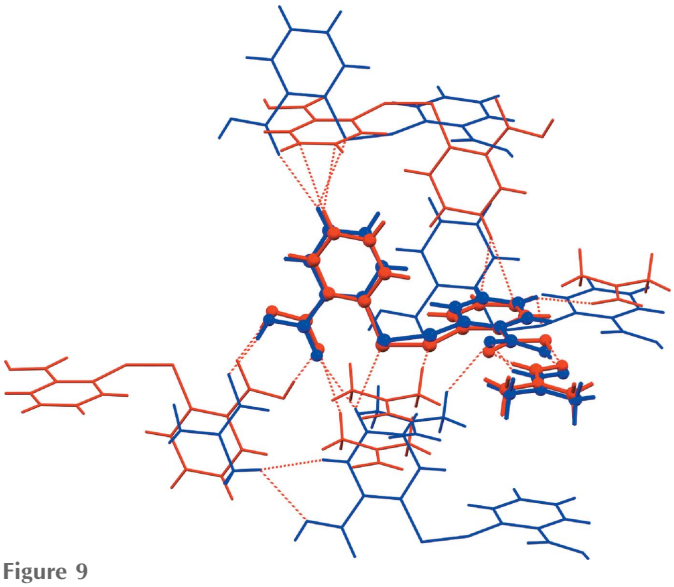

**Figure 9**
A comparison of crystal packing similarity within a 20% geometric tolerance between (I) (red trace) and (II) (blue) with the overlapped molecules represented in ball-and-stick mode.

## 6. Comparison of (I) with the di-DMF solvate

The crystal structure of DTBA·2DMF (II) is also known, being reported four times (XEBDEO: Cai *et al.*, 2006; XEBDEO01: Ma *et al.*, 2013; AYIVAH: Baruah, 2016; CUNJUT: Tan & Tiekink, 2020). The key feature of the molecular packing of (II) is that each carboxylic acid residue of the DTBA acid molecule, which lacks crystallographic symmetry, is hydrogen bonded to a DMF molecule to form a three-molecule aggregate. For comparison purposes, (II) (CUNJUT: Tan & Tiekink, 2020), which was evaluated under similar experimental conditions as (I), was also subjected to molecular packing and contact distribution studies. The calculation of the solvent accessible void space using the parameters as mentioned previously shows that the inclusion of additional DMF molecules in the unit-cell is almost directly proportional to the occupied volume by the solvent molecule, *i.e.* occupied unit-cell volume = 220.8 Å$^3$ = 25.4% for (I) and 526.4 Å$^3$ and 47.5% for (II).

An analysis of the molecular packing similarity between (I) and (II) demonstrates that although the crystal solvates contain DTBA molecule in common, the inclusion of additional DMF results results in a significant deviation in the molecular packing as evidenced in Fig. 9. Here, only two out of 15 molecules in the cluster of molecules being studied are overlapped (within 20% geometric tolerance), with the r.m.s. deviation of the molecular packing being 0.337 Å.

In term of contact distribution on the Hirshfeld surface for the corresponding individual DTBA molecules and overall (I) and (II), it is noted there are no great disparities in the percentage contributions to the calculated surfaces, Fig. 10.

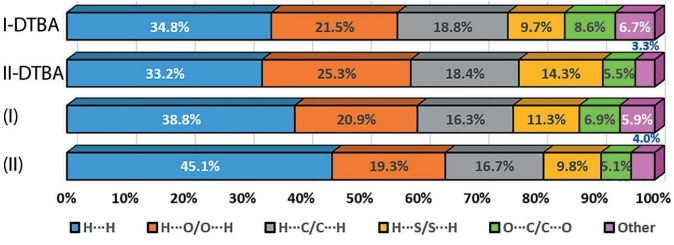


**Figure 10**
A comparison of the percentage contributions of various contacts to the Hirshfeld surfaces for (*a*) DTBA in (I), (*b*) DTBA in (II), (*c*) (I) and (*d*) (II).

## 7. Database survey

As mentioned in the *Chemical Context*, DTBA is usually generated during co-crystallization experiments with 2-mercaptobenzoic acid (2-MBA), implying oxidation of the latter. In addition to oxidation of 2-MBA, other crystallization outcomes have been observed during recent experiments suggesting chemical reactions are occurring. A less common outcome of crystallization experiments with 2-MBA was the sulfur extrusion product, 2,2′-thiodibenzoic acid (Gorobet *et al.*, 2018), obtained during attempts to react 2-MBA with copper(I) chloride in the presence of two equivalents of triphenylphosphane (Tan & Tiekink, 2018). In a series of experiments with the isomeric Schiff bases, *N*,*N*-bis[(pyridine-*n*-yl)methylene]cyclohexane-1,4-diamine, for $n$ = 2, 3 and 4 (Lai *et al.*, 2006), very different products have been characterized from comparable reaction conditions. Referring to Fig. 11, (III) is the $n$ = 4 isomer. Thus, when (III) was co-crystallized with 2-MBA, a salt of composition [1,4-$H_3N^{(+)}C_6H_{10}N^{(+)}H_3$][DTBA_2H]·DMF·$H_2O$ was isolated (KOZSOK; Tan & Tiekink, 2019*f*). A more dramatic outcome was the cation, (IV), in the salt hydrate formulated as (IV)[DTBA_2H]·2$H_2O$, where (IV) is 2-(4-ammoniocyclohexyl)-3-(pyridin-2-yl)imidazo[1,5-*a*]pyridin-2-ium di-cation, isolated from the co-crystallization of 2-MBA with the $n$ = 2 isomer of (III) (TOLLEO; Tan & Tiekink, 2019*e*). When 4-MBA was employed with the $n$ = 2 isomer, [1,4-$H_3N^{(+)}C_6H_{10}N^{(+)}H_3$][4-DTBA_2H]·DMSO·$H_2O$ was the crystallization product (WOVHOH; Tan & Tiekink, 2019*g*). Simple co-crystallization of 4-MBA with the 4-isomer gave the anticipated co-crystal [4-DTBA](II) (GOQREM; Tan & Tiekink, 2019*h*). The aforementioned crystallization outcomes vindicate continued systematic investigations in this field.

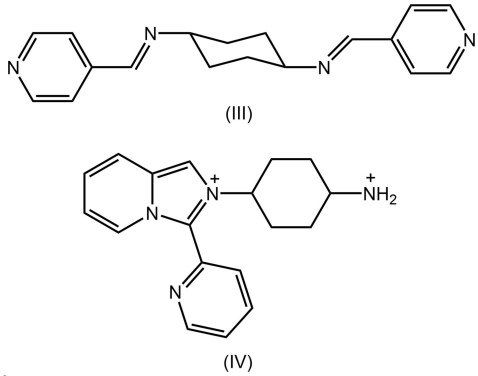


**Figure 11**
Chemical diagrams for (III) and (IV).

**Table 5**
Experimental details.

| | |
|---|---|
| Crystal data | |
| Chemical formula | $C_{14}H_{10}O_4S_2{\cdot}C_3H_7NO$ |
| $M_r$ | 379.43 |
| Crystal system, space group | Triclinic, $P\overline{1}$ |
| Temperature (K) | 100 |
| $a, b, c$ (Å) | 5.05866 (4), 12.2617 (1), 15.1009 (1) |
| $\alpha, \beta, \gamma$ (°) | 106.149 (1), 96.446 (1), 100.884 (1) |
| $V$ (Å$^3$) | 869.94 (1) |
| $Z$ | 2 |
| Radiation type | Cu $K\alpha$ |
| $\mu$ (mm$^{-1}$) | 3.03 |
| Crystal size (mm) | 0.24 × 0.16 × 0.06 |
| Data collection | |
| Diffractometer | XtaLAB Synergy, Dualflex, AtlasS2 |
| Absorption correction | Gaussian (*CrysAlis PRO*; Rigaku OD, 2018) |
| $T_{min}$, $T_{max}$ | 0.316, 1.000 |
| No. of measured, independent and observed [$I > 2\sigma(I)$] reflections | 19670, 3543, 3410 |
| $R_{int}$ | 0.025 |
| (sin $\theta/\lambda)_{max}$ (Å$^{-1}$) | 0.630 |
| Refinement | |
| $R[F^2 > 2\sigma(F^2)]$, $wR(F^2)$, $S$ | 0.026, 0.072, 1.07 |
| No. of reflections | 3543 |
| No. of parameters | 234 |
| No. of restraints | 2 |
| H-atom treatment | H atoms treated by a mixture of independent and constrained refinement |
| $\Delta\rho_{max}$, $\Delta\rho_{min}$ (e Å$^{-3}$) | 0.23, −0.34 |

Computer programs: *CrysAlis PRO* (Rigaku OD, 2018), *SHELXS* (Sheldrick, 2015*a*), *SHELXL2017/1* (Sheldrick, 2015*b*), *ORTEP-3 for Windows* (Farrugia, 2012), *DIAMOND* (Brandenburg, 2006) and *publCIF* (Westrip, 2010).

## 8. Synthesis and crystallization

The DMF monosolvate of DTBA, (I), was obtained by the addition of a small amount of DMF to the benzene solution of 2-mercaptobenzoic acid (1 ml DMF: 5 ml benzene), followed by slow evaporation of the solvent. M.p. 462.5–463.7 K. IR (cm$^{-1}$): 3072 $\nu$(C—H), 1680 $\nu$(C═O), 1464 $\nu$(C═C), 1410 $\delta$(C—H), 722 $\nu$(C—S).

## 9. Refinement

Crystal data, data collection and structure refinement details are summarized in Table 5. The carbon-bound H atoms were placed in calculated positions (C—H = 0.95–0.98 Å) and were included in the refinement in the riding model approximation, with $U_{iso}$(H) set to 1.2$U_{eq}$(C). The oxygen-bound H atoms were located from a difference-Fourier map and refined with O—H = 0.84±0.01 Å, and with $U_{iso}$(H) set to 1.5$U_{eq}$(O).

## Funding information

Crystallographic research at Sunway University is supported by Sunway University Sdn Bhd (grant No. STR-RCTR-RCCM-001-2019).

## References

Baruah, J. B. (2016). Private Communication (refcode: AYIVAH). CCDC, Cambridge England.
Boys, S. F. & Bernardi, F. (1970). *Mol. Phys.* **19**, 553–566.
Brandenburg, K. (2006). *DIAMOND*. Crystal Impact GbR, Bonn, Germany.
Broker, G. A., Bettens, R. P. A. & Tiekink, E. R. T. (2008). *CrystEngComm*, **10**, 879–887.
Broker, G. A. & Tiekink, E. R. T. (2007). *CrystEngComm*, **9**, 1096–1109.
Cai, Y.-P., Sun, F., Zhu, L.-C., Yu, Q.-Y. & Liu, M.-S. (2006). *Acta Cryst.* E**62**, o841–o842.
Chai, J. D. & Head-Gordon, M. (2008). *Phys. Chem. Chem. Phys.* **10**, 6615–6620.
Contreras-García, J., Johnson, E. R., Keinan, S., Chaudret, R., Piquemal, J.-P., Beratan, D. N. & Yang, W. (2011). *J. Chem. Theory Comput.* **7**, 625–632.
Farrugia, L. J. (2012). *J. Appl. Cryst.* **45**, 849–854.
Frisch, M. J., *et al.* (2016). *Gaussian16*, Revision A. 03. Gaussian, Inc., Wallingford, CT, USA.
Gorobet, A., Vitiu, A., Petuhov, O. & Croitor, L. (2018). *Polyhedron*, **151**, 51–57.
Johnson, E. R., Keinan, S., Mori-Sánchez, P., Contreras-García, J., Cohen, A. J. & Yang, W. (2010). *J. Am. Chem. Soc.* **132**, 6498–6506.
Lai, C. S., Mohr, F. & Tiekink, E. R. T. (2006). *CrystEngComm*, **8**, 909–915.
Ma, D., Gao, F. & Niu, D. (2013). *Jiangsu Shifan Daxue Xuebao, Ziran Kexueban* (In Chinese; *J. Jiangsu Normal Univ.*) **31**, 47–51.
Macrae, C. F., Sovago, I., Cottrell, S. J., Galek, P. T. A., McCabe, P., Pidcock, E., Platings, M., Shields, G. P., Stevens, J. S., Towler, M. & Wood, P. A. (2020). *J. Appl. Cryst.* **53**, 226–235.
Nakanishi, W., Nakamoto, T., Hayashi, S., Sasamori, T. & Tokitoh, N. (2007). *Chem. Eur. J.* **13**, 255–268.
Rigaku OD (2018). *CrysAlis PRO* Software system. Rigaku Corporation, Oxford, UK.
Rowland, C. E., Cantos, P. M., Toby, B. H., Frisch, M., Deschamps, J. R. & Cahill, C. L. (2011). *Cryst. Growth Des.* **11**, 1370–1374.
Sheldrick, G. M. (2015*a*). *Acta Cryst.* A**71**, 3–8.
Sheldrick, G. M. (2015*b*). *Acta Cryst.* C**71**, 3–8.
Simon, S., Duran, M. & Dannenberg, J. J. (1996). *J. Chem. Phys.* **105**, 11024–11031.
Spackman, M. A. & Jayatilaka, D. (2009). *CrystEngComm*, **11**, 19–32.
Tan, S. L., Jotani, M. M. & Tiekink, E. R. T. (2019). *Acta Cryst.* E**75**, 308–318.
Tan, S. L. & Tiekink, E. R. T. (2018). *Acta Cryst.* E**74**, 1764–1771.
Tan, S. L. & Tiekink, E. R. T. (2019*a*). *Acta Cryst.* E**75**, 1–7.
Tan, S. L. & Tiekink, E. R. T. (2019*b*). *Z. Kristallogr. New Cryst. Struct.* **234**, 433–436.
Tan, S. L. & Tiekink, E. R. T. (2019*c*). *Z. Kristallogr. New Cryst. Struct.* **234**, 1305–1308.
Tan, S. L. & Tiekink, E. R. T. (2019*d*). *Acta Cryst.* E**75**, 475–481.
Tan, S. L. & Tiekink, E. R. T. (2019*e*). *Z. Kristallogr. New Cryst. Struct.* **234**, 797–799.
Tan, S. L. & Tiekink, E. R. T. (2019*f*). *Z. Kristallogr. New Cryst. Struct.* **234**, 903–905.
Tan, S. L. & Tiekink, E. R. T. (2019*g*). *Z. Kristallogr. New Cryst. Struct.* **234**, 1301–1304.
Tan, S. L. & Tiekink, E. R. T. (2019*h*). *Z. Kristallogr. New Cryst. Struct.* **234**, 1121–1123.
Tan, S. L. & Tiekink, E. R. T. (2020). CSD Communication (CCDC 2002479). CCDC, Cambridge, England. DOI: 10.5517/ccdc.csd.cc256r38
Turner, M. J., McKinnon, J. J., Wolff, S. K., Grimwood, D. J., Spackman, P. R., Jayatilaka, D. & Spackman, M. A. (2017). *Crystal Explorer 17*. The University of Western Australia.
Weigend, F. & Ahlrichs, R. (2005). *Phys. Chem. Chem. Phys.* **7**, 3297–3305.

# supporting information

*Acta Cryst.* (2020). E**76**, 1150-1157 [https://doi.org/10.1107/S2056989020008257]

# 2,2′-(Disulfanediyl)dibenzoic acid *N*,*N*-dimethylformamide monosolvate: crystal structure, Hirshfeld surface analysis and computational study

**Sang Loon Tan and Edward R. T. Tiekink**

## Computing details

Data collection: *CrysAlis PRO* (Rigaku OD, 2018); cell refinement: *CrysAlis PRO* (Rigaku OD, 2018); data reduction: *CrysAlis PRO* (Rigaku OD, 2018); program(s) used to solve structure: *SHELXS* (Sheldrick, 2015*a*); program(s) used to refine structure: *SHELXL2017/1* (Sheldrick, 2015*b*); molecular graphics: *ORTEP-3 for Windows* (Farrugia, 2012), *DIAMOND* (Brandenburg, 2006); software used to prepare material for publication: *publCIF* (Westrip, 2010).

## 2,2′-(Disulfanediyl)dibenzoic acid *N*,*N*-dimethylformamide monosolvate

*Crystal data*

$C_{14}H_{10}O_4S_2{\cdot}C_3H_7NO$
$M_r$ = 379.43
Triclinic, $P\overline{1}$
$a$ = 5.05866 (4) Å
$b$ = 12.2617 (1) Å
$c$ = 15.1009 (1) Å
$\alpha$ = 106.149 (1)°
$\beta$ = 96.446 (1)°
$\gamma$ = 100.884 (1)°
$V$ = 869.94 (1) Å$^3$
$Z$ = 2
$F(000)$ = 396
$D_x$ = 1.449 Mg m$^{-3}$
Cu $K\alpha$ radiation, $\lambda$ = 1.54184 Å
Cell parameters from 13143 reflections
$\theta$ = 3.1–76.0°
$\mu$ = 3.03 mm$^{-1}$
$T$ = 100 K
Prism, colourless
0.24 × 0.16 × 0.06 mm

*Data collection*

XtaLAB Synergy, Dualflex, AtlasS2 diffractometer
Detector resolution: 5.2558 pixels mm$^{-1}$
$\omega$ scans
Absorption correction: gaussian (CrysAlisPro; Rigaku OD, 2018)
$T_{min}$ = 0.316, $T_{max}$ = 1.000
19670 measured reflections
3543 independent reflections
3410 reflections with $I > 2\sigma(I)$
$R_{int}$ = 0.025
$\theta_{max}$ = 76.3°, $\theta_{min}$ = 3.1°
$h$ = −6→6
$k$ = −15→13
$l$ = −18→18

*Refinement*

Refinement on $F^2$
Least-squares matrix: full
$R[F^2 > 2\sigma(F^2)]$ = 0.026
$wR(F^2)$ = 0.072
$S$ = 1.07
3543 reflections
234 parameters
2 restraints
Primary atom site location: dual
Hydrogen site location: mixed
H atoms treated by a mixture of independent and constrained refinement
$w = 1/[\sigma^2(F_o^2) + (0.0405P)^2 + 0.3204P]$ where $P = (F_o^2 + 2F_c^2)/3$
$(\Delta/\sigma)_{max}$ = 0.001
$\Delta\rho_{max}$ = 0.23 e Å$^{-3}$
$\Delta\rho_{min}$ = −0.34 e Å$^{-3}$

*Special details*

**Geometry**. All esds (except the esd in the dihedral angle between two l.s. planes) are estimated using the full covariance matrix. The cell esds are taken into account individually in the estimation of esds in distances, angles and torsion angles; correlations between esds in cell parameters are only used when they are defined by crystal symmetry. An approximate (isotropic) treatment of cell esds is used for estimating esds involving l.s. planes.

*Fractional atomic coordinates and isotropic or equivalent isotropic displacement parameters (Å²)*

| | *x* | *y* | *z* | $U_{iso}$*/$U_{eq}$ |
|---|---|---|---|---|
| S1 | 0.13127 (6) | 0.80270 (2) | 0.28401 (2) | 0.01841 (9) |
| S2 | −0.10332 (6) | 0.84945 (2) | 0.18710 (2) | 0.01848 (9) |
| O1 | 0.32810 (18) | 0.61831 (8) | 0.48410 (6) | 0.02255 (19) |
| H1O | 0.480 (2) | 0.6544 (14) | 0.5192 (11) | 0.034* |
| O2 | 0.42509 (17) | 0.76207 (8) | 0.41991 (6) | 0.02129 (19) |
| O3 | −0.30085 (18) | 0.92323 (8) | −0.07873 (6) | 0.02025 (19) |
| H3O | −0.403 (3) | 0.9709 (12) | −0.0714 (12) | 0.030* |
| O4 | −0.37132 (17) | 0.93328 (7) | 0.06697 (6) | 0.01850 (18) |
| O5 | 0.78590 (18) | 0.72556 (8) | 0.59804 (6) | 0.0248 (2) |
| N1 | 1.1659 (2) | 0.87050 (9) | 0.62312 (7) | 0.0212 (2) |
| C1 | 0.2742 (2) | 0.67339 (10) | 0.42316 (8) | 0.0176 (2) |
| C2 | 0.0090 (2) | 0.61916 (10) | 0.35774 (8) | 0.0170 (2) |
| C3 | −0.0765 (2) | 0.67004 (10) | 0.28992 (8) | 0.0166 (2) |
| C4 | −0.3247 (2) | 0.61624 (11) | 0.22897 (9) | 0.0193 (2) |
| H4 | −0.380732 | 0.647747 | 0.181123 | 0.023* |
| C5 | −0.4903 (2) | 0.51701 (11) | 0.23773 (9) | 0.0213 (3) |
| H5 | −0.660717 | 0.482386 | 0.196749 | 0.026* |
| C6 | −0.4093 (3) | 0.46787 (11) | 0.30573 (9) | 0.0219 (3) |
| H6 | −0.524200 | 0.400478 | 0.311867 | 0.026* |
| C7 | −0.1591 (3) | 0.51829 (11) | 0.36451 (8) | 0.0204 (2) |
| H7 | −0.100899 | 0.483843 | 0.410105 | 0.024* |
| C8 | −0.0191 (2) | 0.77686 (10) | 0.07734 (8) | 0.0165 (2) |
| C9 | −0.0966 (2) | 0.80827 (10) | −0.00313 (8) | 0.0156 (2) |
| C10 | −0.0139 (2) | 0.75656 (11) | −0.08709 (9) | 0.0192 (2) |
| H10 | −0.062982 | 0.779179 | −0.140805 | 0.023* |
| C11 | 0.1383 (3) | 0.67300 (11) | −0.09306 (9) | 0.0222 (3) |
| H11 | 0.196005 | 0.639201 | −0.150100 | 0.027* |
| C12 | 0.2057 (3) | 0.63912 (11) | −0.01461 (9) | 0.0225 (3) |
| H12 | 0.306044 | 0.580290 | −0.018626 | 0.027* |
| C13 | 0.1282 (2) | 0.69023 (11) | 0.06944 (9) | 0.0200 (2) |
| H13 | 0.175946 | 0.665950 | 0.122388 | 0.024* |
| C14 | −0.2676 (2) | 0.89386 (10) | −0.00130 (8) | 0.0152 (2) |
| C15 | 0.9281 (2) | 0.80364 (11) | 0.57469 (9) | 0.0207 (2) |
| H15 | 0.861275 | 0.816264 | 0.517895 | 0.025* |
| C16 | 1.2863 (3) | 0.85536 (13) | 0.70996 (9) | 0.0282 (3) |
| H16A | 1.268974 | 0.919308 | 0.763221 | 0.042* |
| H16B | 1.480062 | 0.855771 | 0.709563 | 0.042* |
| H16C | 1.190793 | 0.780820 | 0.715480 | 0.042* |
| C17 | 1.3127 (3) | 0.96362 (12) | 0.59254 (10) | 0.0281 (3) |

| | | | | |
|---|---|---|---|---|
| H17A | 1.220139 | 0.959343 | 0.530664 | 0.042* |
| H17B | 1.500247 | 0.954934 | 0.588962 | 0.042* |
| H17C | 1.316721 | 1.039287 | 0.637404 | 0.042* |

*Atomic displacement parameters (Å²)*

| | $U^{11}$ | $U^{22}$ | $U^{33}$ | $U^{12}$ | $U^{13}$ | $U^{23}$ |
|---|---|---|---|---|---|---|
| S1 | 0.01995 (15) | 0.01712 (15) | 0.01807 (15) | 0.00257 (11) | −0.00087 (11) | 0.00800 (11) |
| S2 | 0.02349 (16) | 0.01848 (15) | 0.01612 (15) | 0.00924 (11) | 0.00252 (11) | 0.00694 (11) |
| O1 | 0.0220 (4) | 0.0274 (5) | 0.0201 (4) | 0.0019 (4) | −0.0003 (3) | 0.0142 (4) |
| O2 | 0.0223 (4) | 0.0213 (4) | 0.0196 (4) | 0.0009 (3) | −0.0004 (3) | 0.0097 (3) |
| O3 | 0.0250 (4) | 0.0239 (5) | 0.0179 (4) | 0.0124 (4) | 0.0059 (3) | 0.0106 (3) |
| O4 | 0.0215 (4) | 0.0206 (4) | 0.0170 (4) | 0.0096 (3) | 0.0043 (3) | 0.0078 (3) |
| O5 | 0.0235 (4) | 0.0279 (5) | 0.0236 (5) | 0.0015 (4) | 0.0021 (4) | 0.0127 (4) |
| N1 | 0.0222 (5) | 0.0218 (5) | 0.0182 (5) | 0.0039 (4) | 0.0032 (4) | 0.0049 (4) |
| C1 | 0.0207 (6) | 0.0198 (6) | 0.0141 (5) | 0.0069 (5) | 0.0049 (4) | 0.0061 (4) |
| C2 | 0.0181 (6) | 0.0195 (6) | 0.0143 (5) | 0.0054 (4) | 0.0049 (4) | 0.0050 (4) |
| C3 | 0.0166 (5) | 0.0167 (5) | 0.0175 (6) | 0.0056 (4) | 0.0051 (4) | 0.0049 (4) |
| C4 | 0.0181 (6) | 0.0206 (6) | 0.0195 (6) | 0.0071 (5) | 0.0025 (5) | 0.0054 (5) |
| C5 | 0.0167 (5) | 0.0216 (6) | 0.0224 (6) | 0.0036 (5) | 0.0029 (5) | 0.0024 (5) |
| C6 | 0.0224 (6) | 0.0194 (6) | 0.0227 (6) | 0.0012 (5) | 0.0082 (5) | 0.0052 (5) |
| C7 | 0.0250 (6) | 0.0208 (6) | 0.0173 (6) | 0.0053 (5) | 0.0066 (5) | 0.0078 (5) |
| C8 | 0.0148 (5) | 0.0156 (5) | 0.0184 (6) | 0.0026 (4) | 0.0018 (4) | 0.0052 (4) |
| C9 | 0.0130 (5) | 0.0142 (5) | 0.0187 (6) | 0.0018 (4) | 0.0013 (4) | 0.0053 (4) |
| C10 | 0.0184 (6) | 0.0195 (6) | 0.0191 (6) | 0.0034 (4) | 0.0026 (4) | 0.0057 (5) |
| C11 | 0.0214 (6) | 0.0214 (6) | 0.0225 (6) | 0.0067 (5) | 0.0061 (5) | 0.0026 (5) |
| C12 | 0.0195 (6) | 0.0184 (6) | 0.0297 (7) | 0.0082 (5) | 0.0038 (5) | 0.0052 (5) |
| C13 | 0.0188 (6) | 0.0187 (6) | 0.0235 (6) | 0.0056 (5) | 0.0013 (5) | 0.0083 (5) |
| C14 | 0.0146 (5) | 0.0142 (5) | 0.0156 (5) | 0.0010 (4) | 0.0002 (4) | 0.0053 (4) |
| C15 | 0.0215 (6) | 0.0235 (6) | 0.0174 (6) | 0.0059 (5) | 0.0031 (5) | 0.0062 (5) |
| C16 | 0.0279 (7) | 0.0346 (7) | 0.0199 (6) | 0.0089 (6) | −0.0014 (5) | 0.0058 (5) |
| C17 | 0.0282 (7) | 0.0219 (6) | 0.0312 (7) | 0.0004 (5) | 0.0071 (6) | 0.0060 (5) |

*Geometric parameters (Å, º)*

| | | | |
|---|---|---|---|
| S1—C3 | 1.7929 (12) | C6—C7 | 1.3853 (18) |
| S1—S2 | 2.0524 (4) | C6—H6 | 0.9500 |
| S2—C8 | 1.7894 (12) | C7—H7 | 0.9500 |
| O1—C1 | 1.3177 (15) | C8—C13 | 1.3951 (16) |
| O1—H1O | 0.845 (9) | C8—C9 | 1.4103 (16) |
| O2—C1 | 1.2216 (15) | C9—C10 | 1.3988 (16) |
| O3—C14 | 1.3184 (14) | C9—C14 | 1.4772 (15) |
| O3—H3O | 0.845 (9) | C10—C11 | 1.3831 (17) |
| O4—C14 | 1.2295 (14) | C10—H10 | 0.9500 |
| O5—C15 | 1.2423 (16) | C11—C12 | 1.3887 (18) |
| N1—C15 | 1.3228 (17) | C11—H11 | 0.9500 |
| N1—C17 | 1.4557 (17) | C12—C13 | 1.3855 (18) |
| N1—C16 | 1.4573 (17) | C12—H12 | 0.9500 |

| | | | |
|---|---|---|---|
| C1—C2 | 1.4893 (16) | C13—H13 | 0.9500 |
| C2—C7 | 1.3985 (17) | C15—H15 | 0.9500 |
| C2—C3 | 1.4082 (17) | C16—H16A | 0.9800 |
| C3—C4 | 1.3958 (17) | C16—H16B | 0.9800 |
| C4—C5 | 1.3889 (18) | C16—H16C | 0.9800 |
| C4—H4 | 0.9500 | C17—H17A | 0.9800 |
| C5—C6 | 1.3885 (18) | C17—H17B | 0.9800 |
| C5—H5 | 0.9500 | C17—H17C | 0.9800 |

| | | | |
|---|---|---|---|
| C3—S1—S2 | 104.21 (4) | C10—C9—C14 | 118.89 (10) |
| C8—S2—S1 | 104.44 (4) | C8—C9—C14 | 121.39 (10) |
| C1—O1—H1O | 109.1 (12) | C11—C10—C9 | 120.98 (11) |
| C14—O3—H3O | 107.5 (11) | C11—C10—H10 | 119.5 |
| C15—N1—C17 | 121.01 (11) | C9—C10—H10 | 119.5 |
| C15—N1—C16 | 121.21 (11) | C10—C11—C12 | 119.16 (11) |
| C17—N1—C16 | 117.77 (11) | C10—C11—H11 | 120.4 |
| O2—C1—O1 | 123.78 (11) | C12—C11—H11 | 120.4 |
| O2—C1—C2 | 121.86 (11) | C11—C12—C13 | 120.69 (11) |
| O1—C1—C2 | 114.35 (10) | C11—C12—H12 | 119.7 |
| C7—C2—C3 | 119.58 (11) | C13—C12—H12 | 119.7 |
| C7—C2—C1 | 120.03 (11) | C12—C13—C8 | 120.87 (12) |
| C3—C2—C1 | 120.37 (11) | C12—C13—H13 | 119.6 |
| C4—C3—C2 | 118.92 (11) | C8—C13—H13 | 119.6 |
| C4—C3—S1 | 121.24 (9) | O4—C14—O3 | 123.20 (10) |
| C2—C3—S1 | 119.84 (9) | O4—C14—C9 | 122.27 (10) |
| C5—C4—C3 | 120.53 (11) | O3—C14—C9 | 114.53 (10) |
| C5—C4—H4 | 119.7 | O5—C15—N1 | 124.80 (12) |
| C3—C4—H4 | 119.7 | O5—C15—H15 | 117.6 |
| C4—C5—C6 | 120.71 (11) | N1—C15—H15 | 117.6 |
| C4—C5—H5 | 119.6 | N1—C16—H16A | 109.5 |
| C6—C5—H5 | 119.6 | N1—C16—H16B | 109.5 |
| C7—C6—C5 | 119.22 (11) | H16A—C16—H16B | 109.5 |
| C7—C6—H6 | 120.4 | N1—C16—H16C | 109.5 |
| C5—C6—H6 | 120.4 | H16A—C16—H16C | 109.5 |
| C6—C7—C2 | 120.98 (12) | H16B—C16—H16C | 109.5 |
| C6—C7—H7 | 119.5 | N1—C17—H17A | 109.5 |
| C2—C7—H7 | 119.5 | N1—C17—H17B | 109.5 |
| C13—C8—C9 | 118.50 (11) | H17A—C17—H17B | 109.5 |
| C13—C8—S2 | 121.28 (9) | N1—C17—H17C | 109.5 |
| C9—C8—S2 | 120.20 (9) | H17A—C17—H17C | 109.5 |
| C10—C9—C8 | 119.71 (11) | H17B—C17—H17C | 109.5 |

| | | | |
|---|---|---|---|
| O2—C1—C2—C7 | −179.30 (11) | S1—S2—C8—C9 | −166.35 (8) |
| O1—C1—C2—C7 | 0.13 (16) | C13—C8—C9—C10 | −3.03 (17) |
| O2—C1—C2—C3 | −0.45 (17) | S2—C8—C9—C10 | 175.70 (9) |
| O1—C1—C2—C3 | 178.99 (10) | C13—C8—C9—C14 | 176.08 (10) |
| C7—C2—C3—C4 | −1.89 (17) | S2—C8—C9—C14 | −5.18 (15) |
| C1—C2—C3—C4 | 179.25 (10) | C8—C9—C10—C11 | 1.39 (18) |

| | | | |
|---|---|---|---|
| C7—C2—C3—S1 | 177.41 (9) | C14—C9—C10—C11 | −177.74 (11) |
| C1—C2—C3—S1 | −1.45 (15) | C9—C10—C11—C12 | 0.97 (18) |
| S2—S1—C3—C4 | 6.15 (10) | C10—C11—C12—C13 | −1.66 (19) |
| S2—S1—C3—C2 | −173.13 (8) | C11—C12—C13—C8 | −0.04 (19) |
| C2—C3—C4—C5 | 2.79 (17) | C9—C8—C13—C12 | 2.38 (18) |
| S1—C3—C4—C5 | −176.49 (9) | S2—C8—C13—C12 | −176.34 (9) |
| C3—C4—C5—C6 | −1.54 (18) | C10—C9—C14—O4 | 172.13 (11) |
| C4—C5—C6—C7 | −0.67 (18) | C8—C9—C14—O4 | −6.99 (17) |
| C5—C6—C7—C2 | 1.57 (18) | C10—C9—C14—O3 | −7.31 (15) |
| C3—C2—C7—C6 | −0.29 (18) | C8—C9—C14—O3 | 173.56 (10) |
| C1—C2—C7—C6 | 178.58 (11) | C17—N1—C15—O5 | −177.13 (12) |
| S1—S2—C8—C13 | 12.35 (11) | C16—N1—C15—O5 | 1.3 (2) |

*Hydrogen-bond geometry (Å, º)*

*Cg*1 and *Cg*2 are the centroids of the (C2–C7) and (C8–C13) rings, respectively.

| *D*—H···*A* | *D*—H | H···*A* | *D*···*A* | *D*—H···*A* |
|---|---|---|---|---|
| O1—H1*O*···O5 | 0.85 (1) | 1.75 (1) | 2.5981 (13) | 176 (2) |
| O3—H3*O*···O4$^{i}$ | 0.84 (2) | 1.78 (2) | 2.6215 (13) | 175 (2) |
| C15—H15···O2 | 0.95 | 2.38 | 3.1162 (15) | 134 |
| C7—H7···O1$^{ii}$ | 0.95 | 2.53 | 3.2850 (16) | 136 |
| C1—O2···*Cg*1$^{iii}$ | 1.22 (1) | 3.42 (1) | 3.4843 (12) | 83 (1) |
| C14—O4···*Cg*2$^{iv}$ | 1.23 (1) | 3.33 (1) | 3.6227 (12) | 94 (1) |
| C11—H11···*Cg*1$^{v}$ | 0.95 | 2.94 | 3.7962 (14) | 150 |

Symmetry codes: (i) −*x*−1, −*y*+2, −*z*; (ii) −*x*, −*y*+1, −*z*+1; (iii) *x*+1, *y*, *z*; (iv) *x*−1, *y*, *z*; (v) −*x*, −*y*+1, −*z*.